White Rose
university consortium
Universities of Leeds, Sheffield & York

eprints@whiterose.ac.uk
https://eprints.whiterose.ac.uk/

A NOVEL PROGRESSIVE GRID GENERATION METHOD FOR FREE-FORM GRID STRUCTURE DESIGN AND CASE STUDIES

Fengcheng Liu[1,2], Ruoqiang Feng[1*],Konstantinos Daniel Tsavdaridis[2]

[1]The Key Laboratory of Concrete and Prestressed Concrete Structures of Ministry of Education, Southeast University, Nanjing 211189, China

[2]School of Civil Engineering, Faculty of Engineering and Physical Sciences, University of Leeds, Woodhouse Lane, LS2 9JT, Leeds UK

Abstract: Due to its high structural efficiency and aesthetics, free-form grid structures have been widely used in various public structures. However, it is neither a convenient nor an obvious task for engineers to create a discrete grid on a free-form surface that manifests the architect's intent. This paper presents an efficient design approach based on Coulomb's law to generate well-shaped and fluent grids for free-form grid structural design. In the method, nodes of the grid structure are considered to be interacting particles in an electric field and are added to the surface in a progressive way. The nodal position is determined by Monte Carlo simulation and the grid is generated by connecting the particles that are already in equilibrium. According to the different ways of adding particles, two variations of the method are introduced in this paper: point-based progressive method (PBPM), and curve-based progressive method (CBPM). Case studies are provided to demonstrate the effective execution of the proposed method. The results show that the proposed method can effectively avoid mapping distortion and generate grids with regular shape and fluent lines to meet the aesthetic requirements. Furthermore, the proposed method provides flexible control over the direction and size of the grid, which gives architects a more flexible choice.

Keywords: free-form surface; space grid structure; uniform triangular grid; grid generation; Coulomb's law

1. Introduction

The emergence of grid structures is a major step in the development of complex shapes in AEC (Architecture, Engineering, and Construction), according to Du [1]. In recently years, the free-form grid structures have become popular structural typologies thanks to their splendid visual effects and the capacity to cover large spaces with an uninterrupted span, see Fig.1. They are widely used in a variety of building types, such as exhibition pavilions, stadiums, assembly halls, and protective shelters [2]. Compared with the traditional analytic surface grid structure, the shapes of free-form grid structures are more flexible and diverse, and it can better address the needs of architects in the architectural modeling diversification, as discussed by Schlaich [3]. The shape of the grid structure can be obtained by using form-finding techniques like the force density method and the dynamic relaxation method to minimize the amount of material while maximizing the strength [4-8]. However, for a given surface obtained by the form finding method, it is not always an easy task for engineers to determinate the grid layout that respects architectural requirements and is structurally efficient at the same time. In addition, due to the variety of surfaces of the free-form grid structure, the traditional grid generation method has become overextended and difficult to adapt to such structures. Therefore, a practical grid generation method that can quickly generate structural grids that meet the architect's requirements will be necessary, especially in the early design stage.

(a) British Museum Great Court   (b) Singapore's Changi Airport

Fig. 1 Examples of free-form grid structures

Mesh generation started early in the field of Finite Element Analysis (FEA) backed up with fundamental research. Owen [9] systematically summarized the high-quality unstructured meshing algorithm, such as Delaunay Triangulation, the Advancing Front Technique and the Mapping Method, etc. [10-13]. Although the mesh quality required for FEA has much in common with the mesh characteristics required for grid structures, the resulting FEA mesh does not necessarily meet the architect's requirements such as the equal rod length and the architectural grid fluidity.

As for the grid generation methodologies over the free-form surface, generally speaking, topology optimization is one of the effective methods used to create an efficient structural grid on an imposed surface. Peter and Gilbert [14], Paul et al. [15] and Gao et al. [16] have made substantial progress in this area. However, the grid generated via topology optimization is so coarse that it cannot be applied to actual projects directly.

In order to get a practical and efficient grid over a free-form surface, Winslow et al. [17-18] presented a new algorithm that considers the mechanical performance based on a traditional genetic algorithm. Su et al. [19] conducted a similar research and an improved wave-front method was presented to generate better grids on the given surface. According to Su's research, the structural stress trajectory was taken as the direction of the grid advancement. Although the grids obtained by this way have better mechanical performance, the uniformity of the grid is poor, and some distorted unit cells appear.

Actually, one must admit that architects are most concerned about whether the grid has the advantages of fluency and uniformity, and the structural mechanical properties seem to be less important to them. Therefore, many studies have reported the progress of grid generation on a given surface without considering their structural performance. For example, Ding [20] proposed a new method for a free-form surface grid generation, referred to as the iso-parametric line dividing method, which is based on a non-uniform rational B-spline (NRUBS) curve. Wei [21] and Gao [22] proposed a grid generation method over the free-form surface, which combines the surface flattening technique and mapping theory. Shepherd and Richens [23] proposed a Subdivision Surface method, which provides a useful platform for combining creative architectural design with intelligent engineering to produce aesthetically pleasing designs on financially and environmentally limited agendas. Du et al. [1]proposed a specific computing tool to mesh the surface according to the Compass Method, which allows designers to look for optimal mesh orientations regarding the element's curvature. Lefevre et al. [24]used the Compass Method to generate grid shells considering the mechanical performance, while a method with a denser net was presented to improve the grid quality. Taking the roof of the Yas Island Marina hotel as an example, Peng et al. [25] presented a framework to generate mesh patterns that consist of a hybrid of both triangles and quads. Pottmann et al. [26] presented an overview of designing free form grid shells that consist of polyhedral cells or closely related to them.

In research by Persson and Strang [27], an iterative technique was developed for the mesh generation based on a physical analogy between a simplex mesh and a truss structure. Similar to the physical analogy, Shimada and Gossard et al. [28-29] invented an interesting grid generation method called bubble mesh generation. In its actual implementation, the bubble method generated node configurations that yielded virtually no ill-shaped triangles or

tetrahedrals. Wang et al [30-31] extended the bubble grid generation method to the free form curved surface, and proposed a grid generation and optimization framework for the design of free form grid shells. In order to obtain a grid with balanced rod length and fluent lines, Gao et al [32] presented an efficient design tool for the grid generation of free form surface based on the concept of guide lines. Zheleznyakova [33] regarded the grid nodes as interacting particles and developed a new approach for the triangular grid generation based on the molecular dynamics method. Liu et al. [34] proposed an automatic triangular grid generation method for the design of free-form grid structure based on Coulomb's law. With that method, a free-form grid structure with unique topology, where all of the nodes are located at a similar distance to one another can be obtained. However, the drawback of the method is that it is not convenient to control the unit size and the direction of the grid.

In order to generate a grid that satisfies the requirement of uniformity, regularity, and fluidity, and to improve the ability to control the direction and the size of the grid, this paper proposes a progressive grid generation method based on Coulomb's law for the design of free-form grid structure. In this method, the nodes of the spatial structure are considered to be interacted particles in an electric field, and they move towards each other under the drive of the Coulomb force. To ensure that the particles always move on the surface, the attraction of the surface to the particles is introduced, and the particle placement is determined via Monte Carlo simulation. According to the different ways of adding particles, two variations of the method are introduced in this paper: point-based progressive method (PBPM), and curve-based progressive method (CBPM). Several cases are studied to illustrate the execute-ability of this method and the results show that this method can generate grids with excellent quality, and therefore has preferable applicability in the structural concept design stage.

2. Mechanism of the progressive grid generation method
2.1 Driving force and target

Coulomb's Law, which clarifies the law of interaction between charged bodies, was first published in 1784 by French physicist Coulomb. He confirmed that the force of the mutual impact of two electric charges is directly proportional to the product of the value of their charge and inversely proportional to the square of the distance between their middles. The force is along the straight line joining them. If the two charges have the same sign, the electrostatic force between them is repulsive; if they have different signs, the force between them is attractive.

Coulomb's law can be stated as a simple mathematical expression. The vector form of the mathematical equation is:

$$\vec{F} = k \frac{q_1 q_2}{r^2} \vec{r} \tag{1}$$

where q_1, q_2 are the signed magnitudes of the charges, r is the distance between the charges, and k is so-called the factor of proportion expressed in SI system by:

$$k = \frac{1}{4\pi\varepsilon_0} \tag{2}$$

where ε_0 is the intermediate electric constant in the vacuum, therefore k is also a constant.

According to Coulomb's Law, a progressive grid generation method for the free-form grid structure design is developed in this paper. The nodes of the grid structure are considered to be interacting particles in the electric field. The Coulomb force between the charged particles is set as the driving force, which forces the particles to move towards each other. It is assumed that each charged particle has the same value but a different symbol, that is,

$|q_1| = |q_2|$, and then the Coulomb force can be expressed as:

$$F = kQ / r^2 \tag{3}$$

where $Q = |q_1 q_2|$ and q_1, q_2 are the value of the charges, so the value of the Coulomb force in this paper is only related to distance between two charges. For free-form single-layer grid structures, the Coulomb force between two different nodes can be written as:

$$F = 1 / \sqrt{(x_2 - x_1)^2 + (y_2 - y_1)^2 + (z_2 - z_1)^2} \tag{4}$$

where x_i, y_i, z_i are the three-dimensional coordinates of the nodes.

According to the authors' previous research [28], the minimum equivalent field intensity is set as the target and the direction of the electric field intensity is ignored. If i is the source charge that carries a total positive charge Q, the electric field intensity produced at a distance from the source charge r_{ij} is:

$$E_{ij} = k \frac{Q}{r_{ij}^2} \tag{5}$$

The equivalent electric field intensity at node s of the single-layer grid structure can be expressed as:

$$E_s = \sum_{t=1, s \neq t}^{m} E_{st} \tag{6}$$

where m is the number of nodes around the node s, and E_{st} is electric field intensity at node s that is produced by the surrounding node t. In the algorithm, the position of the node is continuously adjusted, once the equivalent electric field intensity satisfies the convergence tolerance, the iteration will be terminated and the nodes will be located at a similar distance to one another.

Although a relatively uniform triangle mesh can be obtained based on the above convergence condition, since the grid generation process is a process of automatic particle organization, the randomness is so strong that the algorithm has a weak ability to control the direction and size of the grid, and unable to meet the architect's requirements for design diversity.

In order to improve the algorithm's ability to control the size of the grid in this paper, the convergence condition is adjusted accordingly, and the equivalent field intensity at node s is defined as:

$$E_s = \sum_{i=1}^{n} (l_i - R)^2 \tag{7}$$

where R is the specified rod length, l_i is the actual rod length, i is the nodes that participate in iteration around the node s, n is the number of nodes participating in the iteration.

2.2 Surface attraction

Due to the effects of the mapping distortion, it is often difficult to generate a relatively uniform grid on a free-form surface by the traditional mapping method. In this paper, the attractiveness of the surface to the particles is

introduced to avoid mapping distortion. Under the effect of surface attraction, the particles will always move over the surface without leaving the surface and no mapping process is needed.

The attraction of the free-form surface to the particles can be expressed as:

$$F_{Si} = k_s d_{s,i} \qquad (8)$$

where $d_{s,i}$ is the shortest distance between the surface and the new position of particle i after deviating from the surface, and k_s is the surface attraction constant. The effect of attraction is to pull the particles that have deviated from the surface back to ensure the particles always move onto the surface.

Therefore, the total force that drives the motion of particle i in the algorithm can be expressed as:

$$F_{hi} = \begin{cases} F_{Ci} + F_{Si} & \text{i is the free point} \\ 0 & \text{i is the anchor point} \end{cases} \qquad (9)$$

where i is the currently active particle, F_{Ci} is the Coulomb force between particle i and particles around it, F_{Si} is the attraction of the surface to particle i.

2.3 Updating of particle coordinates

In Coulomb's Law, if two charges have the same sign, the electrostatic force between them is repulsive; if they have different signs, the force between them is attractive, with the force joining them along a straight line. In the progressive grid generation method, the threshold of inter-particle distance R is introduced, which is the specified rod length. When the distance between two charged particles is less than R, the user defines the two charges to be like-signed, and the Coulomb force F is repulsive. When the distance between the two particles is more than R, the user defines them to have opposite signs, so the Coulomb force, F, is now attractive. As shown in Fig. 2, particle i is the current active particle; its coordinates are taken as the centre of a circular, and the threshold of the inter-particle distance R is used as the radius of the circular. When the particles around i fall within the circular, they will move away from particle i driven by the Coulomb repulsion. When the particles around i fall outside the circular, they will be attracted and move towards particle i under the influence of coulomb attraction. The force is still along a straight line joining the two particles.
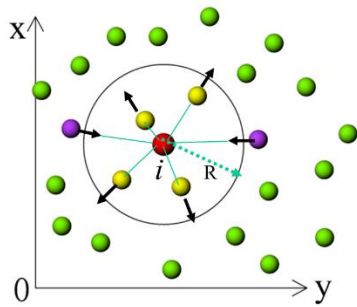

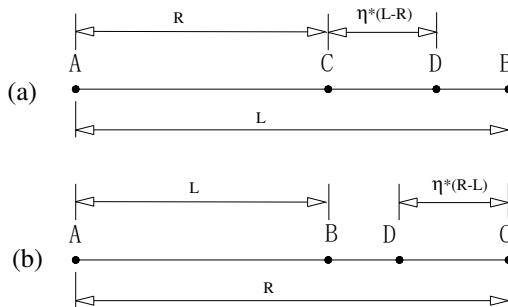Fig.2 Interaction of particles   Fig.3 Schematic updating of particle coordinates

The updated particle coordinates are determined by a statistical sampling-based Monte Carlo (MC) method according to Zhang H [35]. As shown in Fig. 3, A and B are the initial positions of the particles; D is the updated position of the particle; η is the moving coefficient, which is selected according to experience, the best value is between 0 and 0.5; L is the actual distance between the two particles; and R is threshold of inter-particle distance. When the actual distance between the two particles is greater than R, the force between the particles is attractive, so B moves towards A, where CB is the search interval, as shown in Fig. 3 (a). When the actual distance is less than R,

the force is repulsive, so B moves away from A, where BC is search interval, as shown in Fig. 3 (b).

The updated particle coordinates can be expressed as:

$$x_{D,k} = x_{B,k} + \lambda d \tag{10}$$

where $x_{D,k}$ is the updated coordinate of D at the step k, $x_{B,k}$ is the coordinate of B at the step k, λ is the iteration step size and d is the search direction.

2.4 Grid quality evaluation

In general, the quality of the grid can be evaluated easily through a visual check on screen during the grid generation process. However, it is no longer a wise choice for a large-scale free-form grid structure. Therefore, a grid quality criterion become very necessary in order to provide a quantitative evaluation of the generated grid.

It is well known that the grid quality evaluation indicators in the FEM includes the slenderness ratio, taper ratio, internal angle, warpage amount, tensile value, edge node position deviation, etc. However, it is clear that some of these are no longer applicable in the field of free-form grid structure. In practice, it is sometimes more important for the grid structure to generate a grid that has regular shapes and uniform rod lengths.

Therefore, a grid uniformity quality index is used to evaluate the shape and rod length quality in this paper according to [36-37]. While the standard deviation of the rod length is used to evaluate the uniformity of the grids, the shape quality responds to the regularity of the grid.

The standard deviation of the rod length can be defined as:

$$\alpha_l = \sqrt{\sum (l_i - \bar{l})^2 / n} \tag{11}$$

where l_i is the length of rod, $\bar{l}$ is the mean value of the rod length, and n is the number of rods. Because of the existence of dimensions, for structures with different grid sizes, the uniformities of the rods represented by the same standard deviation are also very different. Therefore, some measurements need to be taken to convert it into a dimensionless unit. In this paper, the ratio of the standard deviation α_l to the mean value of rod length $\bar{l}$ was taken as the new uniformity of the grids, which is called the equivalent standard deviation of the rod length in this paper, which is shown as follows:

$$\alpha' = \alpha_l / \bar{l} \tag{12}$$

The shape quality evaluation index of the triangular grid can then be expressed as:

$$Q_t = 4\sqrt{3}A / (l_1^2 + l_2^2 + l_3^2) \tag{13}$$

where A is the area of triangles, and l_1, l_2, l_3 are their side lengths. The value of Q_t is between 0 and 1. A higher value of Q_t means a better shape quality of the grid. When the value of Q_t is 1, the triangle is an equilateral triangle whose shape quality is considered to be the best. When the value of Q_t is 0, it indicates that the triangle has degenerated into a straight line, and the shape quality is the worst.

The shape quality evaluation index of the quadrilateral grid can be defined as:

$$Q_q = 4\sqrt[4]{\frac{S_{\triangle ABC} \times S_{\triangle BCD}}{(l_{AB}^2 + l_{AD}^2) \times (l_{AB}^2 + l_{BC}^2)}} \times \sqrt[4]{\frac{S_{\triangle CDA} \times S_{\triangle ABD}}{(l_{BC}^2 + l_{CD}^2) \times (l_{CD}^2 + l_{AD}^2)}} \tag{14}$$

where the value of Q_q is between 0 and 1, again, higher value of Q_q indicates better shape quality of quadrilateral grids. $S_{\triangle ABC}, S_{\triangle BCD}, S_{\triangle CDA}, S_{\triangle ABD}$ represent the area of the corresponding triangle and $l_{AB}, l_{BC}, l_{AD}, l_{CD}$ represent the corresponding side length of the quadrilateral.

3. Point-based progressive method (PBPM)

PBPM, as the name suggests, it starts from any initial point on the surface and generates a grid in a progressive way by continuously generating random particles around it. This method is suitable for the free-form surfaces with small curvature change, and a highly uniform triangular grid with specified rod length can be obtained.

3.1 Description of algorithm

(a) Grid diffusion   (b) Determination of the new particle
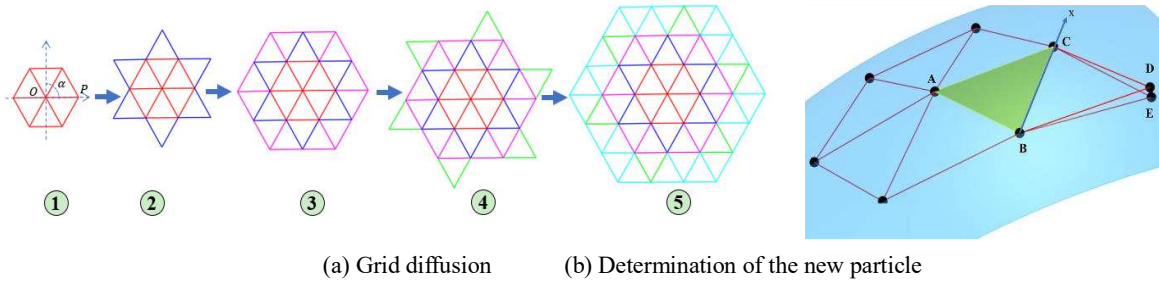
Fig. 4 Grid generation by PBPM

In the PBPM, the grid topological form is predetermined and remains unchanged in the process of grid generation. The grid is generated from a center point and then diffuses outward from the center point in the form of a hexagon, eventually forming a triangular grid, as shown in Fig. 4. The whole process of generation is like covering a space surface with a net. The difference is that the rod length is constantly adjusted by Coulomb's law in the covering process to better close the surface. In specific, the following steps are taken.

Determine the position of the initial point. In general, the position of the initial point can be randomly determined. For a general surface with no overlapping area projected in a certain direction, the initial point is generally selected near the geometric center of the surface; for complex surfaces, an attempt is needed to determine the optimal position of the point.

Generate random points gradually. After the location of the center point is determined, the first-round of random points is generated around it. Then, the points are treated as the charged particles in the electric field and start to move under the combined effect of Coulomb force and surface attractiveness. The equilibrium state is acquired according to the equivalent electric field intensity of each particle and then end the first cycle. Then, fix the equilibrated first-round particles and generate the second-round random points around them, and then start the second cycle. In this way, the final reasonable position of the point can be obtained by cycling in turn.

Generate the whole grid. Connect the optimised particles in the predetermined topological form to generate the final grid.

Moreover, it is worth noting that only the first-round points around the initial point are randomly arranged. Starting from the second-round points, the coordinates of newly added points are determined according to Fig. 4(b). As shown in figure, *A, B,* and *C* are the fixed points, *D* is the newly added point. The initial coordinates of point *D* are determined as follows: first, a working plane is determined by three particles of point *A, B,* and *C*, and then point A is mirrored to get the initial coordinates of point *D* with the symmetrical axis of *BC* connection. Second, point *E* that is on the surface is obtained by pulling point *D* onto the surface by the surface attraction. Finally, Coulomb's law is used to adjust the coordinates of point *E* to get its best position.

In addition, in order to ensure that point *E* does not migrate to the side of point *A* in the process of moving, the

motion range of point E is limited, which is defined as below:

$$l_{DE} \leq k_l R \qquad (15)$$

where the l_{DE} is the distance between D and E, k_l is the distance threshold with the value of 0.5 in this paper, R is the specified rod length.

3.2　Grid direction adjustment

Generally, in order to ensure that the results of the grid generation can better reflect the architectural needs and implications, architects are likely to put forward requirements for grid direction. In PBPM, the grid direction can be adjusted by changing the position of the first-round random points. Specifically, a local coordinate system is established at first, which takes the center point O as the origin and the connection between the center point and any random point P around it as the x-axis, and its vertical direction as the y-axis, as shown in Fig. 4(a). Then, α is introduced as the grid direction adjustment parameter. In the example presented in this paper, $\alpha = 0$ indicates that the x-axis of the local coordinate system is parallel to the x-axis of the global coordinate system. To adjust the direction of the grid, just change the value of α.

3.3　Case study

In this section, the open aluminum alloy lighting roof surface on the upper part of C-shaped column in the terminal building of Beijing Daxing International Airport is taken as an example to illustrate the successful execution of PBPM. Beijing Daxing International Airport Terminal Building, as shown in Fig. 5(a), was designed by British architects Zaha Hadid Architects and French planners ADPI, and executed by the Beijing Institute of Architectural Design (BIAD), was completed on June 30, 2019, and the airport is specified to be open on September 30, 2019. The open aluminum alloy lighting roof was shown in Fig. 5(b), it is an assembled single-layer ellipsoid latticed shell with triangular grids. The grid model of the lighting roof is shown in Fig. 5(c).

(a) Bird's-eye view　　　　　　(b) The lighting roof　　　　(c) Grid model of the lighting roof

Fig. 5 Beijing Daxing International Airport Terminal

At first, determining the position of the initial center point. For this example, the centroid of the surface was chosen as the initial point. Then, the rod length was specified as R=2.0m. Using the PBPM method to generate the triangular grid over the surface, and change the value of α to adjust the direction of the grid. Then, after processing the grids at the boundary manually, the better grids are obtained, as shown in Fig. 6, which is the result of the grids generated in two different directions. It can be seen that the grids obtained by PBPM are not only well-shaped but also have fluent lines, which well embodies the connotation of architecture.
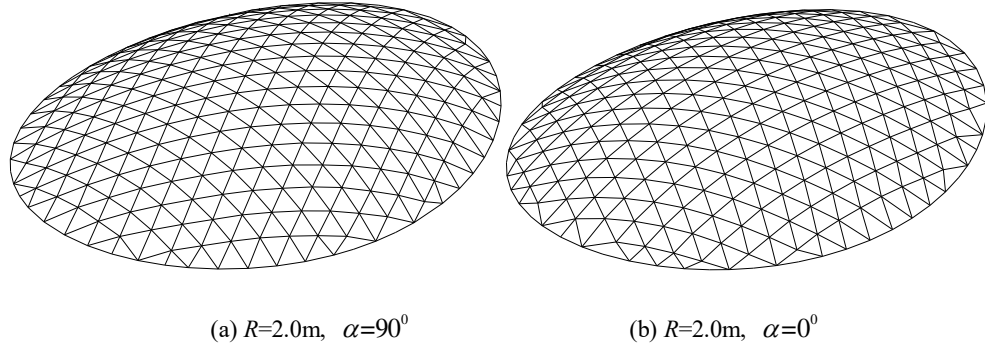
(a) R=2.0m, α=90^0 (b) R=2.0m, α=0^0

Fig. 6 Grid results in different directions

Table 1 Grid quality evaluation of the lighting roof

Model number	Grid type	Rod length		Shape quality index Q_t	
		Mean value (m)	Equivalent standard deviation α'	Mean value (m)	Standard deviation
1	Mapping grid	2.051(2.056)	0.183(0.077)	0.971(0.992)	0.091(0.037)
2	Engineering grid	1.959(2.029)	0.150(0.102)	0.961(0.983)	0.075(0.015)
3	R=2.0m, α=90°	2.020(2.015)	0.109(0.015)	0.983(0.999)	0.073(0.003)
4	R=2.0m, α=0°	2.056(2.009)	0.092(0.032)	0.981(0.998)	0.056(0.006)
5	R=3.0m, α=90°	2.830(2.964)	0.143(0.050)	0.979(0.998)	0.086(0.012)
6	R=3.0m, α=0°	2.878(2.963)	0.100(0.051)	0.974(0.997)	0.074(0.015)
7	R=1.5m, α=90°	1.470(1.49)	0.096(0.020)	0.983(0.999)	0.079(0.003)
8	R=1.5m, α=0°	1.494(1.498)	0.093(0.020)	0.984(0.999)	0.064(0.001)

Note: In parentheses are the data after culling the boundary grid.

     With different specified rod length and different value of α, a diverse range of constructible and visually expressive solutions are obtained, as shown in Table 1. Model 1 is the grid generated by the traditional mapping method; model 2 is the grid in actual engineering; model 3 to model 8 are the results obtained by PBPM after changing the specified rod length and the grid direction. The grid quality indicators of different models as shown in Table 1, include the rod length and the shape quality index. It should be noted that the values in parentheses are results of excluding the rods near the boundary. Since the grid at the boundary is the result of secondary processing such as trimming and extension after the overall grid is generated, eliminating its influence on the algorithm can better reflect the advantages of the progressive grid generation method.

     It can be concluded that although the mapping grid and the grid in practical engineering also have better fluency, the uniformity of the grids is worse than that obtained by PBPM. In specific, when R=2.0m, compared to the grids generated by PBPM, the equivalent standard deviation of the rod length and the standard deviation of shape quality index of model 1 and model 2 are larger, while the mean value of the shape quality index is

smaller. For the grid generated by PBPM, not only the equivalent standard deviation of the rod length is significantly reduced compared with the grid obtained by the mapping method, but also the mean value of the shape quality index is significantly improved. After eliminating the influence of the grid at the boundary, the uniformity of the grids obtained by PBPM is further improved. The equivalent standard deviation of the rod length is reduced by more than 58% compared with the mapping grid, the standard deviation of the shape quality index is reduced by more than 83%, and the mean value is above 0.997. It indicates that the PBPM can effectively avoid the mapping distortion, improve grid quality, and generate more uniform triangular grids. In addition, by comparing the data in Table 1, it can be found that the smaller the specified rod length, the better the uniformity of the grid.
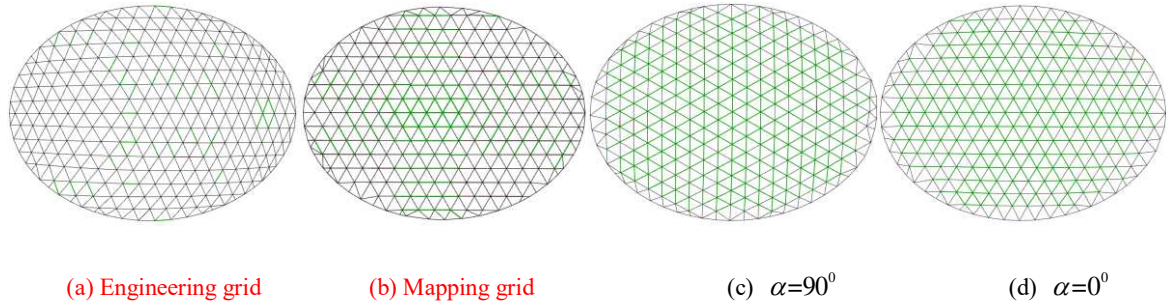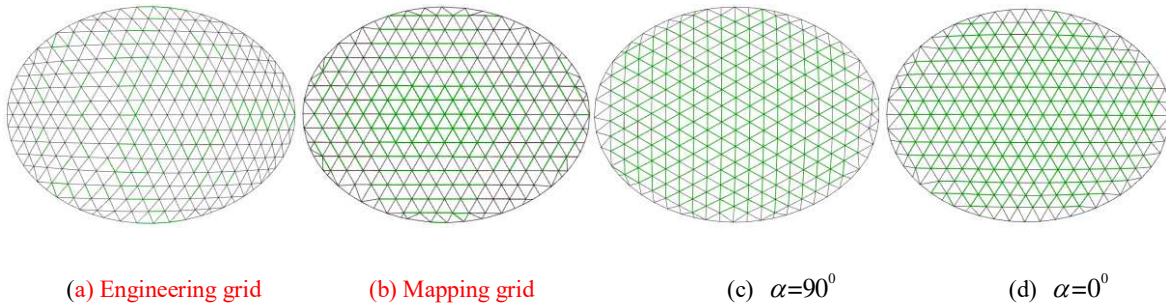

(a) Engineering grid   (b) Mapping grid   (c) $\alpha=90^0$ (d) $\alpha=0^0$

Fig. 7 Rod length distribution of R=2.0m, μ=0.01m

(a) Engineering grid   (b) Mapping grid   (c) $\alpha=90^0$ (d) $\alpha=0^0$

Fig. 8 Rod length distribution of R=2.0m, μ=0.03m

(a) R=3.0m, $\alpha=0^0$ (b) R=3.0m, $\alpha=90^0$ (c) R=1.5m, $\alpha=0^0$ (d) R=1.5m, $\alpha=90^0$

Fig. 9 Rod length distribution in different specified lengths and grid directions (μ=0.01m)

(a) R=3.0m, $\alpha=0^0$ (b) R=3.0m, $\alpha=90^0$ (c) R=1.5m, $\alpha=0^0$ (d) R=1.5m, $\alpha=90^0$
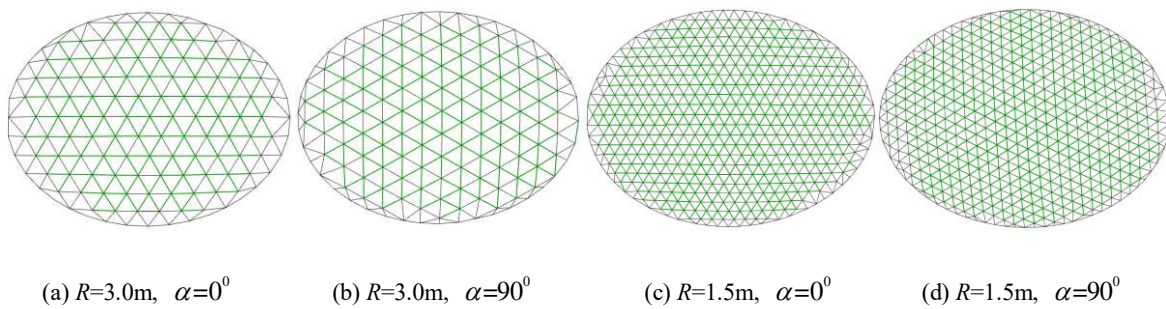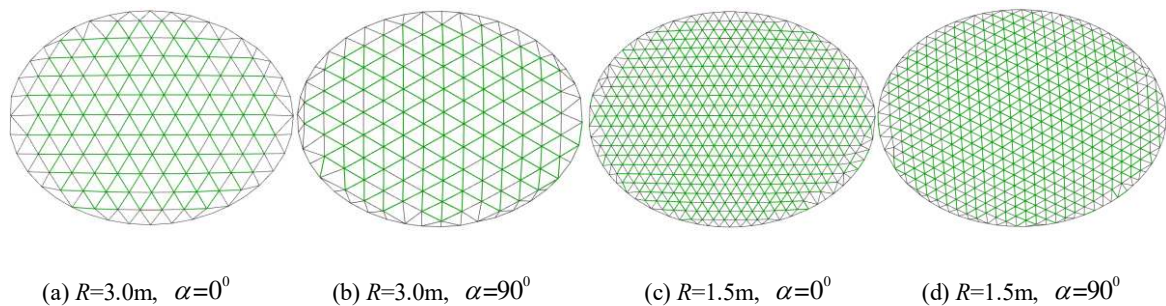
Fig. 10 Rod length distribution in different specified lengths and grid directions ($\mu=0.03m$)

In real-life projects, engineers generally hope that the length specifications (types) of the rods can be as small as possible, which not only facilitates the factory manufacturing, but also facilitates the construction and installation on site. As shown in Fig. 7 to Fig. 10 is the distribution of the rod length in different grids. The rods within the allowable range of different tolerances has been highlighted in green and μ represents the absolute value of the difference between the actual rod length and the specified rod length. It is obvious that the proportion of the rods in the engineering grid that are within the tolerance is the smallest, followed by the grid obtained by the mapping method and the grids obtained by PBPM have the highest proportion. In other words, the engineering grid and the mapping grid have more types of rods, which is adverse to manufacturing and construction ideal approach. It can be seen from the figures that changing the direction of the grid has little effect on the algorithm, and the grids with different directions have a small difference in the proportion of the rods which in the different tolerance.

Table 2 Rod length distribution in different models

Model number	Proportions of rods in different tolerances			
	$\mu=0.01m$	$\mu=0.03m$	$\mu=0.05m$	$\mu=0.08m$
1	17.8%	32.9%	41.8%	51.3%
2	4.7%	14.4%	23.2%	36.8%
3	61.1%	64.2%	69.5%	75.1%
4	60.1%	63.8%	67.5%	73.8%
5	53.9%	59.4%	61.2%	65.3%
6	52.4%	60.5%	60.9%	62.7%
7	64.7%	71.3%	78.6%	86.5%
8	63.1%	70.3%	77.4%	84.9%

The statistical data is presented in Table 2. It can be seen that the proportion of rods in the grids obtained by PBPM that are within the allowable tolerance is much higher than the grids obtained by mapping method and the engineering grid. In model 1, only 17.8% of the rods are in the tolerance when $\mu=0.01m$, and in model 2, the proportion declined to 4.7%. However, the proportion of the rods in model 3 and model 4 which are in the tolerance is more than 60%, indicates that the PBPM can effectively avoid the mapping distortion and generate extremely uniform triangular grids. In addition, with the smaller specified rod length, the higher proportion of the rod in different tolerances is obtained. For this case, when $\mu=0.01m$, the proportion within the tolerance is up to 64.7%, which means that there are more than 60% of the rods in the structure have a length difference of less than 1cm. Therefore, it is completely possible to merge these rods into the same size rods, which greatly facilitates the manufacturing process and at the same time effectively improves the installation efficiency and precision of the grid structure.

3.4 Mechanical performance

Table 3 Comparison between different models

Model number	Model 2	Model 3	Model 4	Decline rate	
Grid type	Engineering grid	$\alpha=90^{o}$	$\alpha=0^{o}$	Model 3 to model 2	Model 4 to model 2
Bearing capacity (N)	8858.57	8726.87	9120.15	1.50%	-2.86%
Total rod length (m)	1604.5	1538.1	1526.1	4.31%	5.13%
Number of triangles	526	483	476	8.1%	9.5%
Number of joints	294	270	267	8.1%	9.1%

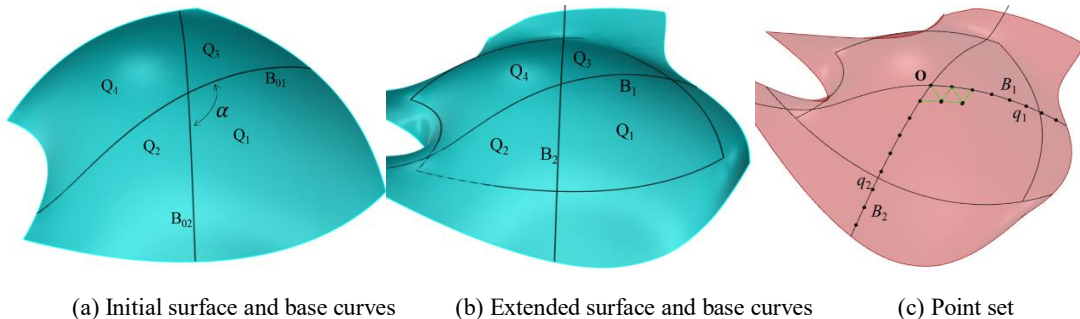| Number of rods	818	751	741	8.2%	9.4%

The grids generated by PBPM have the regular shapes and the fluent lines as well as the great uniformity. However, it is worth understanding the mechanical performance of the grids obtained by PBPM compared to the engineering grid. In general, the aesthetically pleasing attributes of free-form grid structures should boil down to their structural efficiency. A guide to buckling load evaluation of metal reticulated roof structures is present in [38]. Table 3 shows the comparison of the mechanical properties of different models and their various geometrical indicators when R=2.0m. Model 2 is the engineering grid, Model 3 and Model 4 are the grids generated by PBPM with the angle of α=90^0 and α=0^0, respectively. For the ease of calculation, all of the rods are the square steel tubes with dimensions 100 mm×100 mm×4 mm made of Q345 steel. The structural boundary conditions were hinged, and the elastic modulus is $2.0 \times 10^5 MPa$. The dead load of the shell was the building envelope of the roof and the self-weight of the steel tubes. The live load was 0.5kN/m², according to "Load code for the design of building structures" by the Ministry of Construction [39]. It can be seen from the table that the bearing capacity of Model 4 increased by nearly 3% compared to Model 2, while the bearing capacity of Model 3 decreased by only 1.5% compared to Model 2. The reason might be that when specified the α=90^0, there are some small rods near the boundary, which has an adverse effect on the transmission of force.

For other geometrical indicators, in Model 3, the number of triangular roof panels and joints, as well as rods, are reduced by about 8% compared to the actual project, and the total length of the rods is reduced by 4.31%. In Model 4, the number of triangular roof panels and joints, as well as rods, are reduced more than 9% compared to the actual project, and the total length of the rods is reduced by 5.13%. It is imperative to mention that since the Temcor joints are used in this project, the cost of manufacturing and installing the joint is relatively high, which means that the reduction in the number of joints can not only improve the structural construction efficiency but also bring higher economic benefits.

4. Curve-based progressive method (CBPM)

In contrast to PBPM, the CBPM requires the definition of two initial base-curves, which determines the basic direction of the grid. The particles are added to the surface according to the trend of the curve. The CBPM is not only suitable for general curved surfaces but also for curved surfaces with large curvature changes. It has stronger control-ability on the grid direction and can better adapt to the architect's requirements for diversity of grid direction. Therefore, it can better reflect architectural implications and aesthetic feelings.

4.1 Description of algorithm

(a) Initial surface and base curves   (b) Extended surface and base curves   (c) Point set

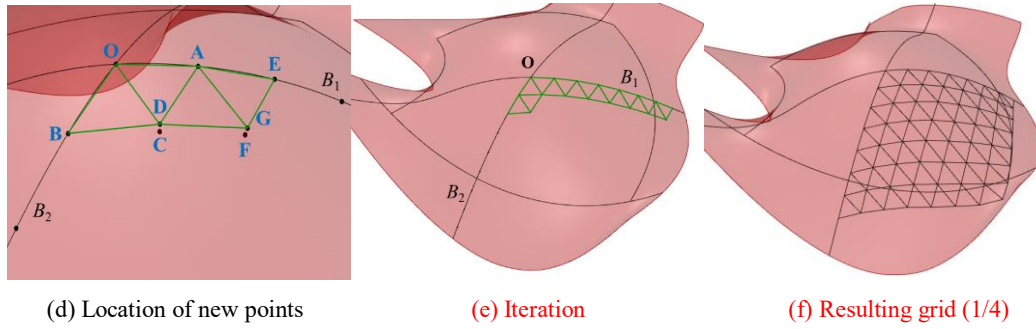|(d) Location of new points | (e) Iteration | (f) Resulting grid (1/4)|

Fig. 11 Main steps of CBPM

Initialization: Two crossing non-uniform rational B-spline (NURBS) curves B_{01} and B_{02} are sketched on the curved surface as the initial base-curves, as shown in Fig. 11(a). Alternatively, the boundaries of the surface, if appropriate, may be selected as the base-curves. Generally, the base-curves are specified by the architect to reflect his architectural design intent. It is worth noting that, in many cases, the grid near the surface boundary does not cover the surface well because the newly added points may fall outside the surface. To solve this problem, the surface and the base-curves should be extended, as shown in Fig. 11(b). In general, the amount of extension is about 2 to 3 times the length of the specified rod length. The two base-curves mark the boundaries of four quarters and start with two consecutive half base-curves, the CBPM is used to sequentially generate the grids in these four sections.

Get the initial point set: Each half-base curve is subdivided into a number of equal (chord) length intervals from the intersection of the two base-curves by the specified rod length. Then point set q_1 and q_2 are obtained, which remains unchanged during the grid generation process, as shown in Fig. 11(c). The program will extract the points in q_1 and q_2 sequentially in the process of grid generation. In the example herein, a grid is first generated along the base-curve B_1.

Generate new points: In CBPM, points are added one by one, so it is a bit time consuming. The way to add points is shown in Fig. 11(d). Point C is the new point, point D is the point obtained by pulling point C back to the surface S by the surface attraction, which is also the point in the algorithm that participates in the iteration. The determination of point C is similar to the PBPM, that is, extracting point O and point A in point set q_1 and point B in point set q_2, and establishing a plane by the three points, then finding the symmetry point of point O on the plane with AB as the axis of symmetry, that is point C.

Iteration: Once the position of point C is determined, it is pulled back to the surface to generate point D. Then, all of the points are considered as charged particles in an electric field, and the equilibrium position of point D is determined by using Coulomb's law. Then, the position of point D remains unchanged, establishing a new plane by point A, point D, and point E, then finding the symmetry point of point A on the plane with DE as the axis of symmetry, that is point F. It is similar to point D that the point G is generated by pulling point F back to the surface. Then, the new iteration begins and the equilibrium position of point G is determined by Coulomb's law. This process is repeated in turn until all points in the point set q_1 are traversed. After the traversal is finished, the points in the point set q_1 is output, and the point B together with the points added in current round are taken as the new point set q_1, and then the second point F of the point set q_2 is substituted for the first point B. Then go into the next cycle until all points in point set q_2 are traversed to complete the grid generation of the first part of the surface. The grid generation of the remaining three parts of the surface is similar to this. The flow chart of CBPM has been shown in Fig. 12.
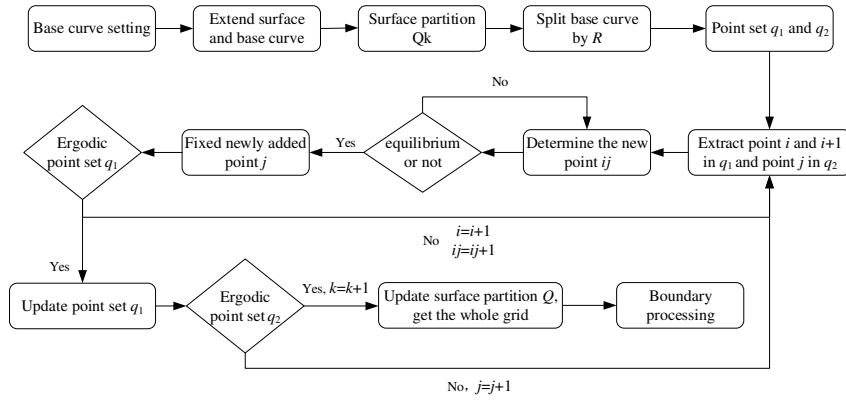
Fig. 12 Flow chart of CBPM

In addition, in the CBPM, the range of motion of the added points is also constrained by formula 15. It is worth mentioning that whether the PBPM or the CBPM, the grid generated in this paper is gradually diffused from the inside of the surface to the boundary, thus ensuring the smoothness and uniformity of the internal grid without considering the effect of the surface boundary. For the grids near the surface boundaries, some manual processing is still needed, like trim the curves near the boundaries and merge nodes with close distances, and so on.

4.2 Case studies

4.2.1 Case one --- a random surface

In this section, the feasibility of CBPM is illustrated by taking the random surface shown in Fig.11 as an example. Two sets of basic-curves with different angles 60° and 90° are adopted respectively, and the specified rod length R is set as 2.5m. The grids obtained by CBPM are shown in Fig. 13. Obviously, all of the grids have smooth lines and the direction of the grid is basically consistent with that of the initial base-curves.
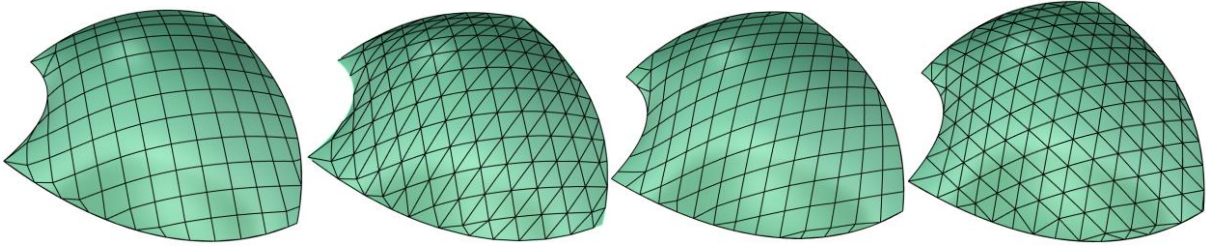
(a) Quadrilateral grid $\alpha = 90^o$ (b) Triangular grid $\alpha = 90^o$ (c) Quadrilateral grid $\alpha = 60^o$ (d) Triangular grid $\alpha = 60^o$

Fig. 13 Grids obtained by CBPM
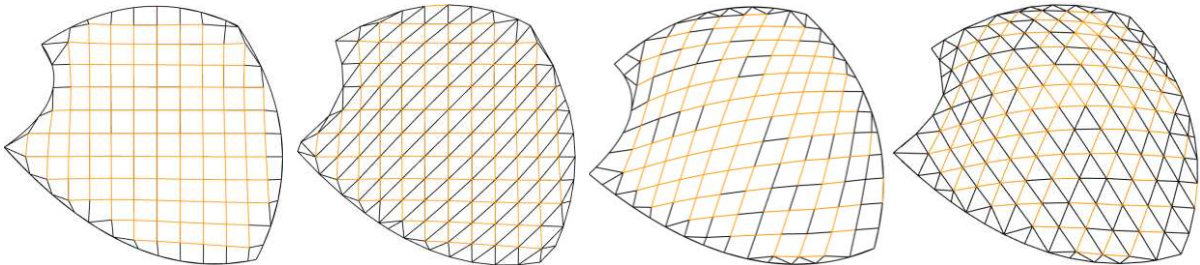
(a) Quadrilateral grid $\alpha = 90^o$ (b) Triangular grid $\alpha = 90^o$ (c) Quadrilateral grid $\alpha = 60^o$ (d) Triangular grid $\alpha = 60^o$

Fig. 14 Rod length distribution in different models (μ=0.01m)

Table 4 Rod length distribution of the random surface

Model number	Grid type	Proportions of rods in different tolerances			
		μ=0.01m	μ=0.03m	μ=0.05m	μ=0.08m

9	quadrilateral grid $\alpha=90^0$, R=2.5m	72.0%	73.2%	74.4%	75.5%
10	triangular grid $\alpha=90^0$, R=2.5m	48.9%	49.7%	50.8%	53.2%
11	quadrilateral grid $\alpha=60^0$, R=2.5m	52.4%	68.0%	70.5%	71.5%
12	triangular grid $\alpha=60^0$, R=2.5m	43.6%	51.7%	54.6%	59.7%

Table 5 Grid quality evaluation of the random surface

Grid type	Rod length		Shape quality index Q_t 和 Q_q	
	Mean value (m)	Equivalent standard deviation α'	Mean value (m)	standard deviation
quadrilateral grid $\alpha=90^0$, R=2.5m	2.48(2.50)	0.13(0.0001)	0.96(0.99)	0.11(0.006)
triangular grid $\alpha=90^0$, R=2.5m	2.70(2.81)	0.21(0.16)	0.84(0.89)	0.11(0.037)
quadrilateral grid $\alpha=60^0$, R=2.5m	2.49(2.50)	0.12(0.004)	0.88(0.89)	0.05(0.041)
triangular grid $\alpha=60^0$, R=2.5m	2.47(2.51)	0.14(0.04)	0.96(0.99)	0.09(0.009)

Note: In parentheses are the data after culling the boundary grid.

When $\mu=0.01m$, the rod length distribution in different models is shown in Fig. 14. It can be seen that when $\alpha=90^o$, an extremely uniform quadrilateral grid is obtained by CBPM, in which the proportion of rods that meet the tolerance $\mu=0.01m$ is as high as 72%, as shown in Table 4. When $\alpha=60^o$, the CBPM generates a uniform triangular grid and the mean value of shape quality index reaches 0.99 without considering the influence of the boundary rods, as shown in Table 5. Among the four grids, the lowest proportion of rods that meet the tolerance is 43.6%, which suggest that more than 40% of the rods in the whole structure can be classified into one group. It is to say, as the type of rod in the structure is reduced, it will undoubtedly be more conducive to improving the efficiency and accuracy of the processing and manufacturing of the rods and the construction of the structure.

4.2.2   Case two --- Admirant entrance building

In PBPM, the grid is generated from a center point, and then diverged outward from the point in the form of a hexagon, eventually forming a triangular grid. If the surface has an obvious shrinkage section or the curvature changes substantially, the grid will intersect itself during iteration, which leads to the failure of grid generation. Therefore, for some surfaces with a significant shrinking cross section in a certain direction, such as the surface shown in Fig. 15, the PBPM usually cannot get better results. However, the CBPM is more adaptable, less affected by the curvature of the surface, and has better control-ability on the direction of the grid, so it can get a high-quality building grid smoothly.

The surface shown in Fig. 15 is a sketch of the Admirant entrance building in Holland, which is designed by M. Fuksas [40]. It is similar to a precious 'jewel' that attracts the public's attention and leads pedestrians into the heart of the building. Similarly, two different layouts of base-curves with the angle of 60º and 90º are adopted in this section respectively.

As shown in Fig. 15(a), the result obtained by the traditional mapping method, that is, directly projecting a quadrilateral grid on a plane onto the given surface. It is clear to see that due to the influence of the mapping

distortion, the quality of the obtained grid is very poor, and the rod length is too long to meet the architect's requirements. Fig. 15(b) and Fig. 15(c) are the grids obtained by the map-guideline method according to Gao et al.[22], which combines the mapping method and the guideline method. The specific process is to first arrange a certain number of straight lines according to a certain distance on a plane, then map the straight lines to the given surface, and then the obtained curves on the surface are divided into equal parts according to a certain distance or number of segments. Finally, the grid is obtained by connecting the split points. Anyway, a mapping process is still needed in this method, so it still cannot better avoid the errors caused by mapping distortion. In addition, at both ends of the surface, the grid is severely clustered, resulting in a very narrow grid and serious degradation in grid quality.
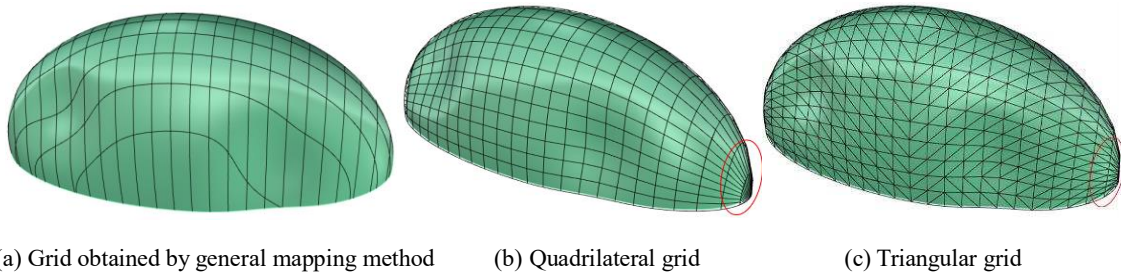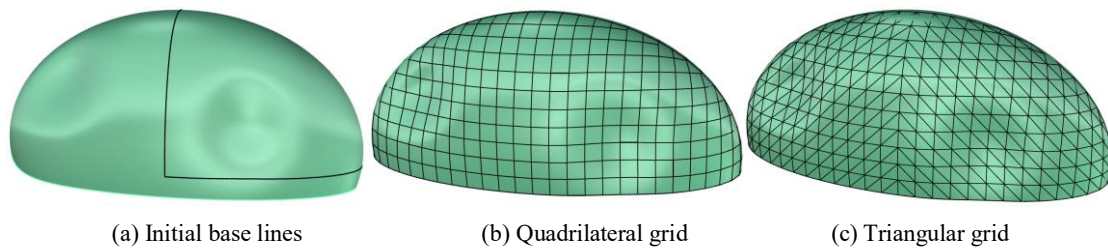

(a) Grid obtained by general mapping method   (b) Quadrilateral grid   (c) Triangular grid

Fig. 15 The grids generated by mapping method

(a) Initial base lines   (b) Quadrilateral grid   (c) Triangular grid

Fig. 16 The grids generated by CBPM (R=2.1m, $\alpha = 90^{o}$)

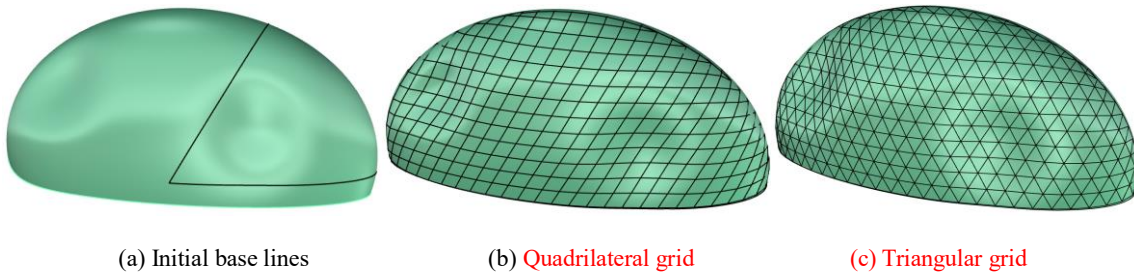(a) Initial base lines   (b) Quadrilateral grid   (c) Triangular grid

Fig. 17 The grids generated by CBPM (R=2.1m, $\alpha = 60^{o}$)

Table 6 Grid quality evaluation of Admirant entrance building

Model number	Grid type	Rod length		Shape quality index Q_t 和 Q_q	
		Mean value (m)	Equivalent standard deviation α'	Mean value	Standard deviation
13	quadrilateral grid α=90°, R=2.1m	2.10	0.077	0.99	0.033
14	quadrilateral grid, mapping method	1.92	0.361	0.826	0.253
15	triangular grid α=60°, R=2.1m	2.34	0.167	0.89	0.151
16	triangular grid, mapping method	2.17	0.333	0.75	0.223
17	quadrilateral grid α=60°, R=2.1m	2.09	0.082	0.89	0.059
18	triangular grid α=60°, R=2.1m	2.11	0.099	0.97	0.064

As shown in Fig. 16 and Fig. 17, the grids obtained by CBPM not only have smooth lines but also have a relatively uniform size, and in addition, there is no grid accumulation at the end of the curved surface. The grid quality evaluation results of the different models are shown in Table 6. Compared with the map-guideline method, when $\alpha = 90^o$, the equivalent standard deviation of the rod length of the quadrilateral grid generated by the CBPM decreases by 78.67% and the standard deviation of the shape quality index decreases by 86.9%, which indicates that the CBPM has effectively avoided the mapping distortion and generated a relatively uniform grid. When the direction of the base-curves is changed, a triangle grid with better uniformity is obtained by CBPM. The standard deviation of shape quality index of the grid decreases by 57.6% compared with that when the angle of the base-curves is 90°.

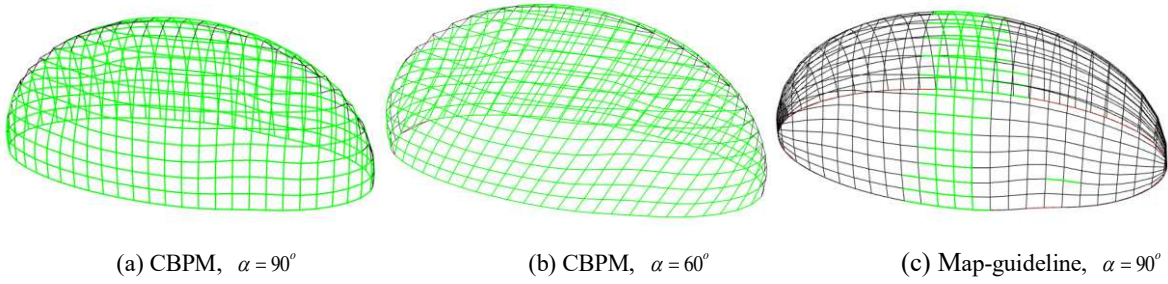(a) CBPM, $\alpha = 90^o$ (b) CBPM, $\alpha = 60^o$ (c) Map-guideline, $\alpha = 90^o$

Fig. 18 Rod length distribution (μ=0.01m, quadrilateral grids)

(a) CBPM, $\alpha = 90^o$ (b) CBPM, $\alpha = 60^o$ (c) Map-guideline, $\alpha = 90^o$
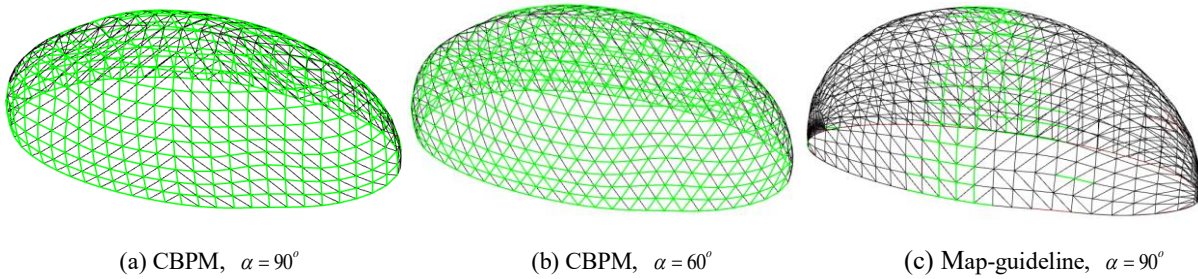
Fig. 19 Rod length distribution (μ=0.01m, triangular grids)

The rod length distribution of the different grids when μ=0.01m is shown in Fig. 18 and Fig. 19. It is obvious to see that most of the rods in the grids generated by CBPM are very close to the specified rod length, while only a few rods in the grids obtained by map-guideline method are close to the specified rod length. To be more precise, the proportion of the rods that meets the tolerance (μ=0.01m) reaches 88.5% in the quadrilateral grids generated by the CBPM, which is also more than 60% in the triangular grids generated by the CBPM. That reveals that a very uniform grid can be obtained by CBPM, which greatly reduces the diversity of the rods in the grid structure. In contrast, as shown in the figures, in the quadrilateral grid obtained by the map-guideline method, only 13.4% of the rods meet the tolerance of μ=0.01m, while only 9.3% in the triangular grid. Besides, from Table 6, it can be seen that the grids obtained by the map-guideline method have relatively poor uniformity, which will inevitably lead to an increase in the diversity of the rods. With the increase of rod diversity, it will undoubtedly increase the construction difficulty of the grid structure, reduce its installation efficiency, and increase some unnecessary capital investment.

4.2.3   Case three --- a parabolic shell
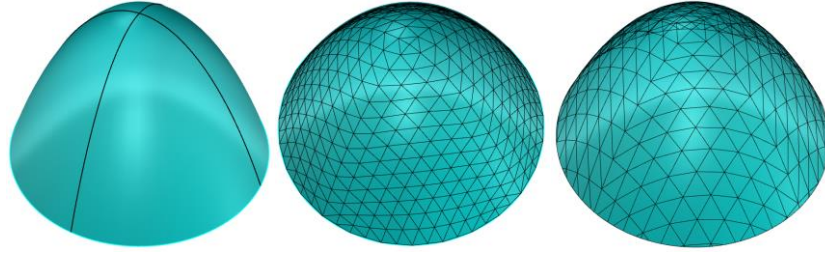
(a) Initial base lines   (b) Grid obtained by CBPM   (c) Grid obtained by mapping method

Fig. 20 Base curves and result grids (R=2.5m, $\alpha = 90^{o}$)
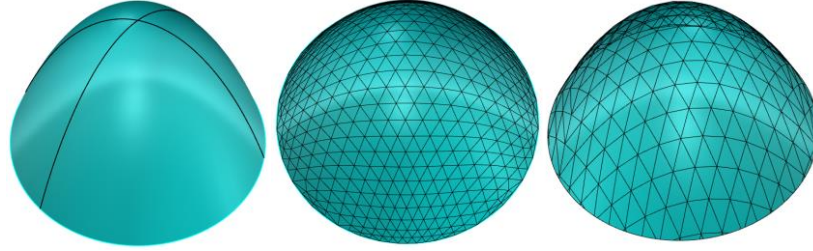
(a) Initial base lines   (b) Grid obtained by CBPM   (c) Grid obtained by mapping method

Fig. 21 Base curves and result grids (R=2.5m, $\alpha = 60^{o}$)

Fig. 20(b) and Fig. 21(b) are the grids generated on a parabolic shell with a large local curvature by CBPM in different grid directions, while Fig. 20(c) and Fig. 21(c) are the grids obtained by the mapping method in the corresponding directions. The grid quality is evaluated by the indices presented in this paper, as shown in table 7. The results show that when $\alpha = 90^{o}$, the equivalent standard deviation of the rod length of the grid generated by CBPM is 0.084, which is decreased by 71.1% compared with that of the grid obtained by mapping method, and the standard deviation of shape quality index is 0.021, which is 72.4% lower than that of the mapping method. When $\alpha = 60^{o}$, in the grid generated by CBPM, the equivalent standard deviation of the rod length is reduced by 64.2% compared with that of the grid obtained by mapping method, and the standard deviation of shape quality index is 56.0% lower than that of the mapping method. It is indicated again that the grids generated by CBPM can effectively avoid the mapping distortion, and a more uniform and fluent construction grid can be obtained.

4.3 Grid size control

Whether it is PBPM or CBPM, the grid size can be changed by specifying different initial rod lengths as needed, which provides architects with more flexible options. In order to adjust and control the size of the grid, it is necessary to modify the specified rod length R and construct a new function.

For PBPM, the constructed function can be expressed as:

$$R_k = k_k R \tag{16}$$

where k represents the kth iteration step, k_k represents the scaling factor, which can be changed by an equal difference series or a geometric series or according to the curvature of the surface, and the user can also customize its value. When k_k =1, it means that the specified rod length is not changed in the process of grid generation.

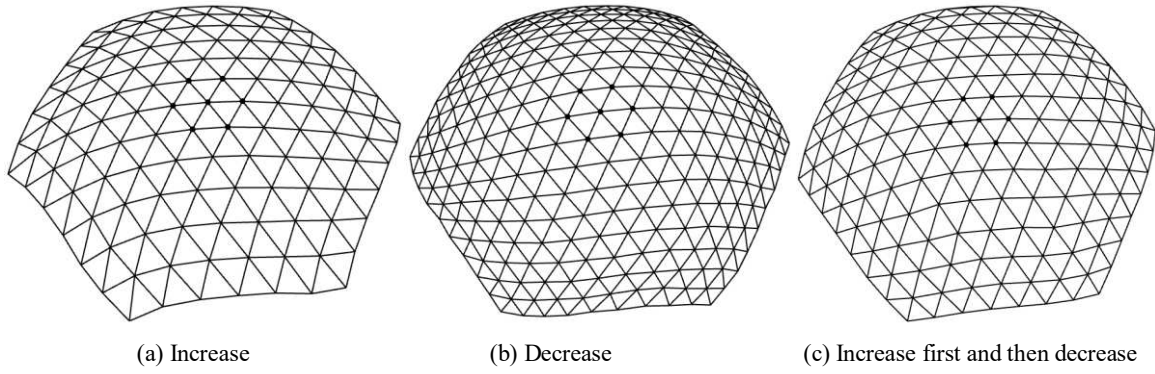| (a) Increase | (b) Decrease | (c) Increase first and then decrease |

Fig. 22 Grids obtained by changing k_k

Fig. 22 is the grids obtained by changing the k_k . It can be seen that the generated grids are regular in shape, controllable in size and well-spaced in density, which provides a reference for the design of grid structure.

For CBPM, the constructed function can be defined as

$$R_{ij} = k_i k_j R \tag{17}$$

where i represents the ith point on the base curve B_1, j represents the jth point on the base curve B_2, k_i and k_j are the scaling factors, which is similar to k_k , and they can also change in the form of an equal difference series or a geometric series. Of course, users can also change their values according to their own needs. When $k_i = k_j = 1$, it means the specified rod length remains constant during the grid generation, which will result in a uniform quadrilateral or triangular grid.
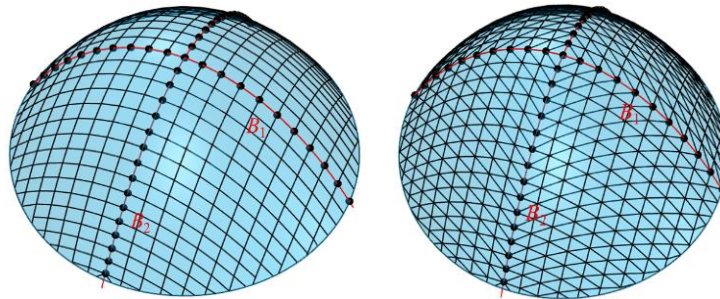
| (a) Quadrilateral grid | (b) Triangular grid |

Fig. 23 The grids obtained by changing k_i
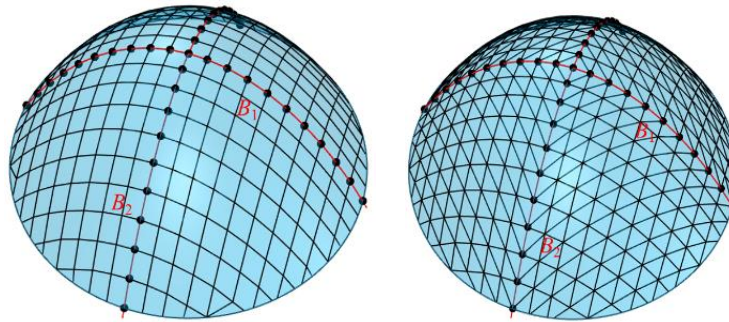
| (a) Quadrilateral grid | (b) Triangular grid |

Fig. 24 The grids obtained by changing k_i and k_j

The grids shown in Fig. 23 are the results by only changing k_i, in this case, k_i is changed in the form of an equal difference series. In the grid generation process, the rod length on curve B_2 remains unchanged, while the rod length on curve B_1 is constantly increasing. As shown in Fig. 24, the grids are obtained by changing k_i and k_j at the same time in the form of an equal difference series. It can be seen that the closer to the boundary, the larger the grid size, but still maintains the smooth lines.

Therefore, in the progressive grid generation method, the grid size adjustment can be achieved conveniently by adjusting the value of the specified rod length R. Then, the architectural grid with natural dimensional variations can be obtained, which improves the flexibility of grid designs while having certain application prospects.

5. Concluding remarks

This paper proposed a novel progressive grid generation methodology for the design of free-form grid structures based on Coulomb's Law. The paper shows how the nodes were added to the surface in a progressive way and treated as the charged particles in an electric field. Then the particles move towards each other under the drive of the Coulomb force and the surface attraction, and the position is determined via Monte Carlo simulation. Consequently, well-shaped grids are obtained by connecting the particles to each other.

Two variations of the progressive grid generation method are presented; the PBPM, where the grid is generated from a center point and then diverged outward from the center point in the form of a hexagon, and the CBPM, where two base-curves are used and the grid is obtained along the curves. Consequently, the PBPM yields extremely uniform triangular grids, while the CBPM results in uniform quadrilateral grids - which optionally can be subdivided into triangular grids.

Some practical case studies for both the PBPM and CBPM are provided. With the ability to control the direction and the size of the grids, the progressive grid generation method can get a diverse range of constructible and visually expressive solutions. The results also indicate that the progressive grid generation method can efficiently reduce the mapping distortion, and the generated grids not only meet the requirements of regularity and fluidity but also embody the architectural connotation.

References
1. Du Peloux L, Baverel O, Caron J F, et al. From shape to shell: a design tool to materialize freeform shapes using gridshell structures. 2013.
2. Iuorio, O., Homma, E. and Tsavdaridis, K.D. The Application of Free-Form Grid Shells as Protective Shelters in Archeological Sites. International Association for Shell and Spatial Structures Symposium (IASS 2016).2016, 26-30 September, Tokyo, Japan.
3. J.Schlaich, H.Schober. Recent glass roofs. Journal of the International Association for Shell and Spatial Structures, 1999, 40(3): 193-205.
4. Schek H J. The force density method for form finding and computation of general networks. Computer methods in applied mechanics and engineering, 1974, 3(1): 115-134.

5. Day A. An introduction to dynamic relaxation. The Engineer, 1965, 219:218–21.

6. Adriaenssens S M L, Barnes M R. Tensegrity spline beam and grid shell structures. Engineering structures, 2001, 23(1): 29-36.

7. Ali N B H, Rhode-Barbarigos L, Smith I F C. Analysis of clustered tensegrity structures using a modified dynamic relaxation algorithm. International Journal of Solids and Structures, 2011, 48(5): 637-647.

8. Hawdon-Earl, S. and Tsavdaridis, K.D. Form Finding and Dimensioning of Reinforced Concrete Shell Roof for Akrotiri (Santorini). Journal of the International Association for Shell and Spatial Structures (IASS).2018, 59(4), 198.

9. Owen S. A survey of unstructured mesh generation technology// 7th International Meshing Roundtable. Berlin: Springer-Verlag, 1998, 239-267.

10. Wang B, Khoo B C, Xie Z Q, et al. Fast centroidal Voronoi Delaunay triangulation for unstructured mesh generation. Journal of Computational & Applied Mathematics.2015, 280: 158-173.

11. Muylle, J., P. Iványi and B. Topping. A new point creation scheme for uniform Delaunay triangulation. Engineering Computations 2002, 19(6): 707-735.

12. Lo S H. Dynamic grid for mesh generation by the advancing front method. Computers & Structures.2013, 123(1): 15-27.

13. Cuillière J C. An adaptive method for the automatic triangulation of 3D parametric surfaces. Computer-Aided Design.1998, 30(2): 139-149.

14. Park P, Gilbert M, Tyas A, et al. (2012) Potential use of structural layout optimization at the conceptual design stage. International Journal of Architectural Computing.2012, 10(1): 13-32.

15. Shepherd P, Pearson W. Topology optimization of algorithmically generated space frames. Proceedings of the IASS symposium. 2013.

16. Zhao X, Miao C, Gao B, et al. Optimization design research of free-form structures based on robustness. Journal of Building Structures, 2014, 6: 019.

17. Winslow P, Pellegrino S, Sharma S B. Mapping two-way grids onto free-form surfaces. Journal of the International Association for Shell and Spatial Structures, 2008, 49(2): 123-130.

18. Winslow P, Pellegrino S, Sharma S B. Multi-objective optimization of free-form grid structures. Structural and multidisciplinary optimization, 2010, 40(1-6): 257.

19. Su L, Zhu S, Xiao N, et al. An automatic grid generation approach over free-form surface for architectural design. Journal of Central South University, 2014, 21(6): 2444-2453.

20. Ding H. Research and implementation of grid design method for free-form grid structures. Zhejiang University. 2014.

21. Dajie W, Ganping S. Mesh generation and optimization method for free-form surface grid. Building Structure, 2013, 19: 013.

22. Gao B, Hao C, Li T, et al. Grid generation on free-form surface using guideline advancing and surface flattening method. Advances in Engineering Software, 2017, 110: 98-109.

23. Shepherd P, Richens P. The case for subdivision surfaces in building design. Journal of the International Association for Shell and Spatial Structures, 2012, 53(4): 237-245.

24. Lefevre B, Douthe C, Baverel O. Buckling of elastic grid shells. Journal of the International Association for shell and spatial structures, 2015, 56(3): 153-171.

25. Peng C H, Pottmann H, Wonka P. Designing patterns using triangle-quad hybrid meshes. ACM Transactions on Graphics, 2018, 37(4CD):1-14.

26. Pottmann H, Jiang C, H?Binger M, et al. Cell packing structures. Computer-Aided Design, 2015, 60:70-83.

27. Persson P O, Strang G. A simple mesh generator in MATLAB. SIAM review, 2004, 46(2): 329-345.

28. Shimada K, Gossard D C. Automatic triangular mesh generation of trimmed parametric surfaces for finite element analysis. Computer Aided Geometric Design, 1998, 15(3): 199-222.

29. Zhou Y, Nie Y, Zhang W. A modified bubble placement method and its application in solving elliptic problem with discontinuous coefficients adaptively. International Journal of Computer Mathematics, 2017, 94(6): 1268-1289.

30. Wang Q S, Ye J, Wu H, et al. A triangular grid generation and optimization framework for the design of free-form grid shells.

Computer-Aided Design, 2019, 113:96-113.

31. Wang Q, Gao B, Wu H. Triangular mesh generation on free-form surfaces based on bubble dynamics simulation. Engineering Computations, 2019, 36(2):646-663.

32. Gao B, Li T, Ma T, et al. A Practical Grid Generation Procedure for the Design of Free-form Structures. Computers & Structures, 2017, 196(FEB.): 292-310.

33. Zheleznyakova A L. Molecular dynamics-based triangulation algorithm of free-form parametric surfaces for computer-aided engineering. Computer Physics Communications, 2015, 190: 1-14.

34. Liu F, Feng R. Automatic triangular grid generation on a free-form surface using a particle self-organizing system. Engineering with Computers, 2020, 36, 377–389.

35. Zhang H, Smirnov A V. Node placement for triangular mesh generation by Monte Carlo simulation. International Journal for numerical methods in engineering, 2005, 64(7): 973-989.

36. XU, Z. H. C. Y. J., Guang, C. D. S. J. Triangulation of Arbitrary Planar Domains Based on Local Priority. Journal of Computer Aided Design & Computer Graphics, 2000, 8: 000.

37. Field D A. Qualitative measures for initial meshes. International Journal for Numerical Methods in Engineering, 2000, 47(4): 887-906.

38. Iass W G. 8. Guide to buckling load evaluation of metal reticulated roof structures (Draft). Rep. Activities IASS WG, 2014, 8(8–10): 57-69.

39. Ministry of Construction. Load code for the design of building structures. GB50009-2012. Beijing; China Architecture & Building Press1. 2012.

40. Fuksas M. The Future Is Now? Parametric Design and Technology in Design Process. Oz, 2016, 38(1): 8.